Low-pressure phase diagram of crystalline benzene from quantum Monte Carlo

Sam Azadi[*]

Department of Physics and Astronomy,

University College London, Thomas Young Center,

London Centre for Nanotechnology,

London WC1E 6BT, United Kingdom

R. E. Cohen

Extreme Materials Initiative, Geophysical Laboratory,

Carnegie Institution for Science, Washington DC, 20015,

USA; Department of Earth- and Environmental Sciences,

Ludwig Maximilians Universität, Munich 80333,

Germany; and Department of Physics and Astronomy,

University College London, London WC1E 6BT, UK

(Dated: July 20, 2016)

Abstract

We studied the low-pressure (0 to 10 GPa) phase diagram of crystalline benzene using quantum Monte Carlo (QMC) and density functional theory (DFT) methods. We performed diffusion quantum Monte Carlo (DMC) calculations to obtain accurate static phase diagrams as benchmarks for modern van der Waals density functionals. Using density functional perturbation theory, we computed the phonon contributions to the free energies. Our DFT enthalpy-pressure phase diagrams indicate that the $Pbca$ and $P2_1/c$ structures are the most stable phases within the studied pressure range. The DMC Gibbs free-energy calculations predict that the room temperature $Pbca$ to $P2_1/c$ phase transition occurs at 2.1(1) GPa. This prediction is consistent with available experimental results at room temperature. Our DMC calculations give 50.6±0.5 kJ/mol for crystalline benzene lattice energy.

1

I. INTRODUCTION

Molecular crystals, including organic and inorganic, are vital in understanding the physics and chemistry of the Earth and planets. They are also of considerable technological interest. Low-Z molecular systems are among the most abundant in the solar system, as represented by planetary gases and ices. Their behaviour at high pressures is crucial in modelling the structure, dynamic, and evolution of the large planets. Moreover, compression of molecular systems provides the opportunities to form new materials, possibly with novel properties, such as high-temperature superconductivity and disordered and amorphous materials. One of the simplest organic molecular solids is crystalline benzene with aromatic van der Waals (vdW) interactions. Given its simplicity, high symmetric, and rigid molecular structure, crystalline benzene has become the model structure for calculating the lattice model vibrations in molecular crystals. Benzene has been extensively studied theoretically and experimentally[1–4]. However, the phase transitions and intermolecular interactions are still controversial. The main goal of this paper is to present a comprehensive study of the phase transition of crystalline benzene at low pressures.

Early experiments by Bridgman[5] revealed that liquid benzene crystallises at 68 MPa with $Pbca$ space group symmetry and closest $C - C$ intermolecular distance of 3.5 $\mathring{A}$. This structure, also, was confirmed at zero pressure and 270 K[6,7]. This phase I is also stable at lower temperatures of 218 and 138 K[8]. Since then, two experimental phase diagrams have been proposed for crystalline benzene. First, based on the phase diagram suggested by Thiéry and Léger[1], liquid benzene crystallises at room temperature and pressure 700 bar within an orthorhombic structure $Pbca$, which is labeled as phase I. Phase II was suggested to exist between 1.4 and 4 GPa. Phases I and II primitive unit cells contain four benzene molecules (Z=4). Phase III is stable between 4 and 11 GPa. The symmetry of phase III is $P2_1/c$ with two benzene molecules per monoclinic primitive unit cell (Z=2). Second, the phase diagram developed by Ciabini et $al.$[9,10] which based on it phase I is orthorhombic $Pbca$ Z=4 and phase II is monoclinic $P2_1/c$ Z=2[3]. Their results are obtained by means of infrared spectroscopy and X-ray analysis under high pressure. The $P2_1/c$ phase is stable up to pressures $20-25$ GPa. This phase diagram only consists of two phases (I and II), and this same result has been reported by other experiments[11]. Katrusiak et al[11], have determined the crystal structures of phases I and II at 295 K. The results of their study confirm Ciabini

et al.'s phase diagram and show that the structures of phases I and II are *Pbca* Z=4 and $P2_1/c$ Z=2, respectively. The results also indicate the absence of other benzene phases in the pressure range up to 5 GPa.

The crystalline benzene phase diagram is a challenge for first-principles theory because the energy differences are insignificant, and they are governed by vdW interactions. The energy difference between crystalline benzene and its low-energy polymorphs under pressure is less than few kJ/mol. Metadynamics calculations predict seven phases[4] as phases I (*Pbca* Z=4), I′ (*Cmca* Z=4), II ($P4_32_12$ Z=4), III ($P2_1/c$ Z=2), III′ ($C2/c$ Z=4), IV (*Pbam* Z=4), and V ($P2_1$ Z=2). In their calculations, they have used numerous randomly generated metastable crystal structures as starting points for the metadynamics. A few metadynamics steps are often sufficient to obtain a more stable structure, which most of the time is similar to *Pbca* Z=4 or $P2_1/c$ Z=2. Density functional theory (DFT) has also been used to compute the lattice energy of crystalline benzene[12,13]. Wen *et al.* employed DFT formalism and used Perdew-Burke-Ernzerhof (PBE)[14] exchange correlation functionals to study the phase diagram of crystalline benzene up to 300 GPa[2]. They explained the complexities observed in benzene at high pressure. In the moderate pressure regime (P < 20 GPa), they found that the *Pbca* structure is stable up to 4 GPa, the $P4_32_12$ phase is preferred in the pressure range of 4−7 GPa, and the $P2_1/c$ structure shows the lowest enthalpy at higher pressures. Therefore, they labelled the *Pbca*, $P4_32_12$, and $P2_1/c$ structures as phases I, II, and III, respectively. The present study shows that the $P4_32_12$ structure is unstable in the pressure range of 0−10 GPa. Thus, the *Pbca* and $P2_1/c$ structures are labelled as phases I and II, respectively.

Recently, quantum chemistry methods have been applied to benzene to obtain sub-kilojoule/mole accuracy in the lattice energy for crystalline benzene[15]. Tremendous measures are necessary to obtain such accuracy. In this work, we will show that QMC is an alternative efficient approach to achieve or surpass such accuracy in benzene crystals, as we previously demonstrated for the benzene dimer[16].

Quantum Monte Carlo (QMC), which approximately solves the electronic Schrödinger equation stochastically[17], can yield highly accurate energies for atoms[18,19], molecules[20–22], and crystals[23–25]. Previous studies have shown that diffusion quantum Monte Carlo (DMC) can provide accurate energies for noncovalent interactions systems[26–30]. DMC can also produce an accurate description of the phase diagram of materials under pressure[31–33]. In

general, QMC-based methods are faster than the most accurate post-Hartree-Fock schemes for large number of particles N. The computational cost of QMC methods scales usually as N^3-N^4 depending on the method.

We have demonstrated that QMC can provide chemical accuracy for the benzene dimer system[16]. We have found optimal variational quantum Monte Carlo (VMC) and DMC binding energies of $-2.3(4)$ and $-2.7(3)$ kcal/mol. The best estimate of the CCSD(T)/CBS limit is $-2.65(2)$ kcal/mol[34]. The consistency among our results, experiments, and quantum chemistry methods, is an important sign of the capability of the QMC-based methods to provide an accurate description of weak intermolecular interactions based on vdW dispersive forces.

In this study, we examine the Z=4 to Z=2 phase transition of crystalline benzene at low pressures. We consider the *Pbca* and $P4_32_12$ structures as best candidates for Z=4 and the $P2_1/c$ structure for Z=2. We study pressures below 10 GPa. We obtain static and dynamic phase diagrams where the phonon contribution to the free energy is included. We employ different vdW functionals[35] and compare them with conventional DFT functionals. We perform QMC calculations to obtain the static enthalpy-pressure phase diagram of crystalline benzene. We will show that DMC provides accurate results for the phase diagram of crystalline benzene.

II.   COMPUTATIONAL DETAILS

Given that the energy differences between crystalline benzene structures are small, the calculations must be performed with the highest possible numerical precision. Our DFT calculations were carried out within the pseudopotential and plane-wave approach using the Quantum ESPRESSO suite of programs[36]. All DFT calculations used ultrasoft pseudopotentials[37]. Pseudopotentials were obtained by PBE[14] exchange correlation functionals. We used a basis set of plane waves with an energy cutoff 100 Ry. Geometry and cell optimisations employed a dense $12 \times 12 \times 12$ **k**-point mesh. The quasi-Newton algorithm was used for cell and geometry optimisation, with convergence thresholds on the total energy and forces of 0.01 mRy and 0.1 mRy/Bohr, respectively, to guarantee convergence of the total energy to less than 1 meV/proton and the pressure to less than 0.1 GPa/proton.

To include the effects of zero point energy (ZPE), vibrational frequencies were calculated

using density-functional perturbation theory as implemented in Quantum ESPRESSO[36]. The ZPE per proton at a specific cell volume V was estimated within the quasi-harmonic approximation: $E_{ZPE}(V) = \hbar\overline{\omega}/2$, where $\overline{\omega} = \sum_{\mathbf{q}} \sum_{i=1}^{N_{mode}} \omega_i(\mathbf{q})/(N_{\mathbf{q}} N_{mode})$. N_{mode} and $N_{\mathbf{q}}$ are the numbers of vibrational modes in the simulation cell and phonon wave vectors $\mathbf{q}$, respectively, and the summation over $\mathbf{q}$ includes all $\mathbf{k}$-points on a $2 \times 2 \times 2$ grid in the Brillouin zone.

The thermodynamic properties are determined by the Helmholtz free energy $F = E - TS$. The free energy can be written as the sum of an electronic and a vibrational term. The electronic entropy is negligible for insulators: $F_{el} \simeq E_{el}$. In our calculations, the electronic part E_{el} is obtained using the DMC method. Thus, the main quantity to calculate for obtaining the thermal properties and finite temperature phase diagram is the vibrational free energy F_{ph}. We use quasi-harmonic approximation to calculate the vibrational free energy[38]:

$$F_{ph}(T, V) = k_B T \sum_{i,\mathbf{q}} ln\{2sinh[\hbar\omega_{i,\mathbf{q}}(V)/2k_B T]\}, \tag{1}$$

where k_B, V, and $\omega_{i,\mathbf{q}}$ are Boltzmann constant, unit cell volume, and eigenvalue of the phonon Hamiltonian, respectively. The pressures P are calculated from the Helmholtz free energies by $P = -(\partial F/\partial V)_T$

We used the CASINO code[39] to perform fixed-node DMC simulations with a trial wave function of the Slater-Jastrow (SJ) form:

$$\Psi_{SJ}(\mathbf{R}) = \exp[J(\mathbf{R})] \det[\psi_n(\mathbf{r}_i^\uparrow)] \det[\psi_n(\mathbf{r}_j^\downarrow)], \tag{2}$$

where $\mathbf{R}$ is a $3N$-dimensional vector of the positions of the N electrons, $\mathbf{r}_i^\uparrow$ is the position of the i'th spin-up electron, $\mathbf{r}_j^\downarrow$ is the position of the j'th spin-down electron, $\exp[J(\mathbf{R})]$ is a Jastrow factor, and $\det[\psi_n(\mathbf{r}_i^\uparrow)]$ and $\det[\psi_n(\mathbf{r}_j^\downarrow)]$ are Slater determinants of spin-up and spin-down one-electron orbitals. These orbitals were obtained from PBE-DFT calculations performed with the plane-wave-based Quantum ESPRESSO code[36], employing Trail-Needs[40,41] Hartree-Fock pseudopotentials. We evaluated the total energy in DMC using the localization approximation[42]. For the QMC study of C and CH-based systems, the Hartree-Fock description of the core is more accurate[43]. A detailed study of silicon also showed[44] that Hartree-Fock provides the most accurate description of the core density compared with generalised gradient approximation and local density approximation (LDA).

We selected a very large basis-set energy cutoff of 200 Ry to approach the complete basis-set limit[45]. The plane-wave orbitals were transformed into a localised "blip" polynomial basis[46]. Our conventional Jastrow factor consists of polynomial one-body electron-nucleus, two-body electron-electron, and three-body electron-electron-nucleus terms, the parameters of which were optimised by minimising the variance of the local energy at the VMC level[47,48]. Our DMC calculations were performed at two different time steps 0.01 and 0.02 a.u. The target population control is two times larger for time step 0.02 a.u. We extrapolated our DMC energies to zero time step using a linear fitting.

III. RESULTS AND DISCUSSION

A. Geometry Analysis

In this section we discuss the results of our geometry optimization. We study the evolution of benzene molecule distances by increasing the pressure. The structure optimization results are compared with experiments.

The primitive unit cells of the $Pbca$, $P4_32_12$, and $P2_1/c$ structures of solid benzene contain four, four, and two benzene molecules, respectively, as shown in figure 1. The $Pbca$ and $P4_32_12$ structures have orthorhombic and tetragonal primitive unit cells, respectively, whereas the $P2_1/c$ primitive unit cell is monoclinic.

For geometry analysis of Z=4 and Z=2 structures, we focus on the $Pbca$ and $P2_1/c$. We will show in the next section that these two structures are the best candidates for the phases I (Z=4) and II (Z=2). Our structure optimization indicates that the molecular orientations do not change significantly within the studied pressure range. We calculated the distances between C atoms on nearest-neighbour (nn) benzene molecules. The nn $C-C$ distances between molecules as function of pressure are reported in figure 2. The nn $C-C$ distances for $Pbca$ and $P2_1/c$ structures are calculated using vdW[50,52] and conventional DFT functionals.

The vdW functionals, particularly vdW-DF2[50], nn $C-C$ distances are in good agreement with experiment[9,10]. The differences between vdW-DF1[52] and vdW-DF2[50] nn $C-C$ distances reduce with increasing pressure. The PBE nn $C-C$ distances are close to vdW functional results at lower pressures, whereas the differences between PBE and vdW results increases
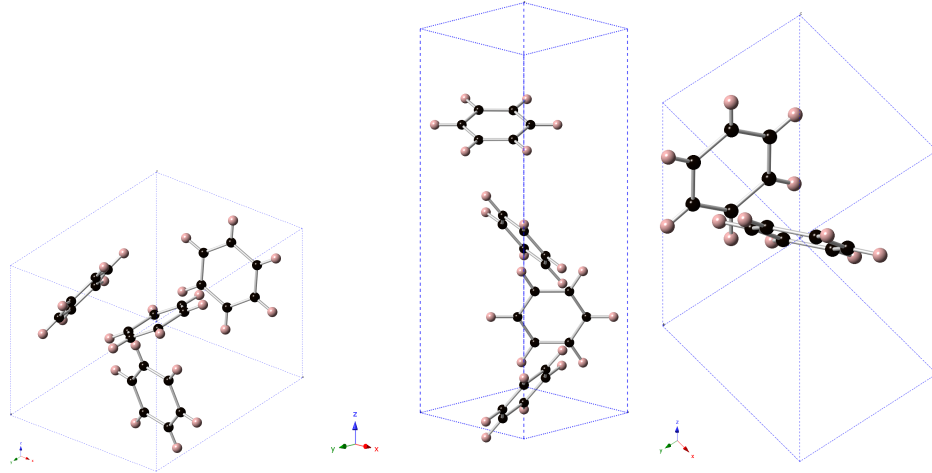
FIG. 1. (colour online) unit cells of the *Pbca* (left), $P4_32_12$ (middle), and $P2_1/c$ (right) structures of solid benzene at low-pressure range. The *Pbca* and $P4_32_12$ primitive unit cells contain four benzene molecules (Z=4), whereas the $P2_1/c$ structure has two benzene molecules (Z=2) in a monoclinic primitive unit cell.

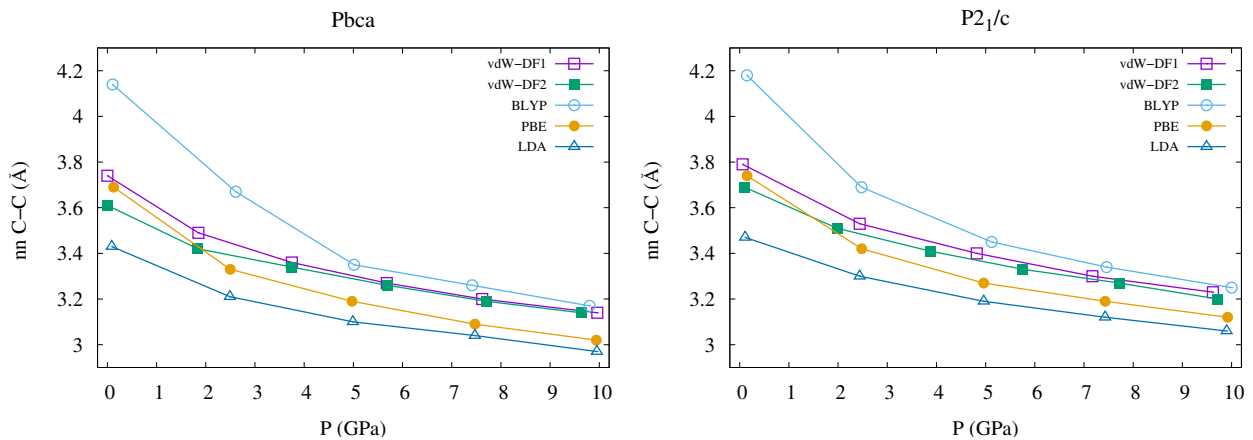FIG. 2. (colour online) Pressure evolution of nearest-neighbour (nn) C−C distances for *Pbca* and $P2_1/c$. The results are obtained by vdW and conventional functionals.

with increasing pressure. The PBE nn C−C distances at higher pressures are close to LDA results. The BLYP nn C−C distances are the largest at low pressures. However, BLYP nn C−C distances are more similar to vdW results at pressures larger than 5 GPa.

The van der Waals radius of Carbon atom r_{WC} is 1.7 Å. In crystalline benzene the benzene molecules are held together by van der Waals forces. The nearest that two C atoms belonging to different benzene molecules can approach each other is estimated by the sum of r_{WC}. We calculated the difference between nearest-neighbour (nn) C−C distances and the
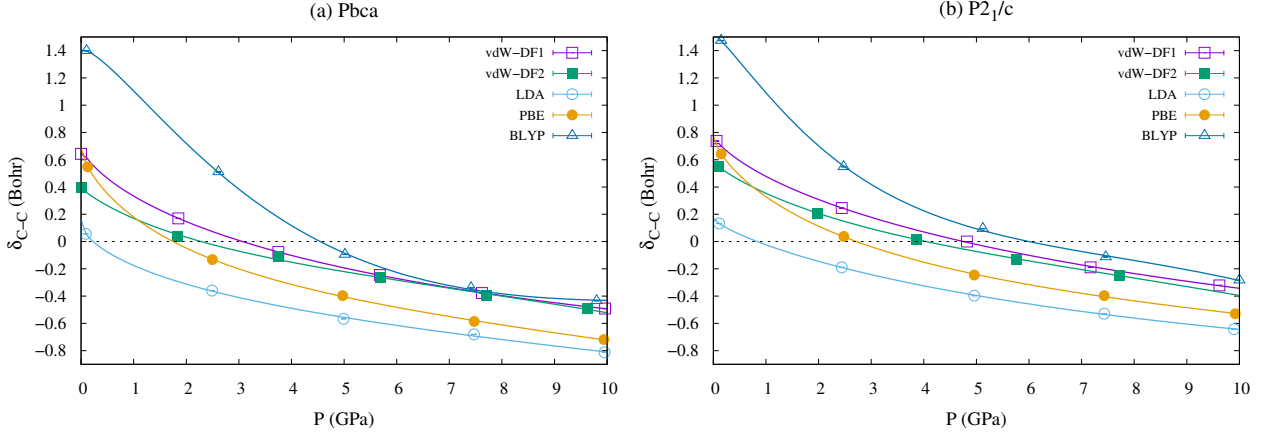
7

FIG. 3. (colour online) Pressure evolution of the difference between nearest-neighbour (nn) C−C distances and the sum of van der Waals radii of C atoms (δ_{C-C}). The results are obtained for *Pbca* and *P*2$_1$/*c* structures using vdW and conventional functionals.

sum of r_{WC} (δ_{C-C}). Figure 3 illustrates δ_{C-C} for *Pbca* and *P*2$_1$/*c* structures. The results are obtained by vdW and conventional functionals. At the same pressure, all the functionals give larger δ_{C-C} for *P*2$_1$/*c* structure. Our EOS calculations, which are presented in figure 7, indicate that at the same pressure molecular density of *P*2$_1$/*c* is larger than *Pbca*. LDA and BLYP provide the smallest and largest δ_{C-C}. Consequently they yield the smallest and largest vdW radii for C atom. Unlike the other functionals, the BLYP δ_{C-C} decline rapidly with increasing the pressure. According to LDA, *Pbca* results, benzene molecules are strongly bonded at pressures larger than 0.2 GPa. In lower pressures PBE δ_{C-C} is close to δ_{C-C} obtained by vdW functionals. With increasing the pressure PBE results become closer to LDA. According to vdW-DF1 results, the benzene molecules in *Pbca* structure is bonded above 3 GPa. Whereas vdW-DF2 results indicate that bonding between benzene molecules in *Pbca* phase could happen around 2 GPa. Based on the experimental phase digram[9,10], the *Pbca* phase is stable at pressures below 1.4 GPa. Our vdW δ_{C-C} results show that there are no strong bonds between benzene molecules in *Pbca* phase. In the *Pbca* structure the benzene molecules only interact through weak dispersive forces.

B. Ground State DFT Phase Diagram

We begin our phase diagram study by DFT enthalpy-pressure calculations at zero temperature. We first present our static phase diagram results where the BornOppenheimer
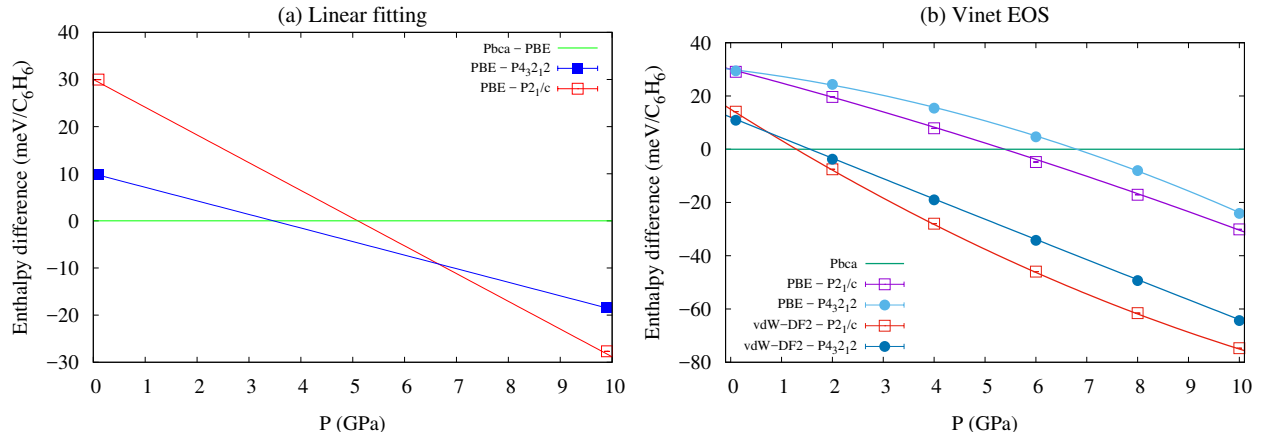
8

FIG. 4. (colour online) Enthalpy difference between the *Pbca*, $P4_32_12$, and $P2_1/c$ structures as function of applied pressure. (a) The results are calculated using PBE and linear fitting on two enthalpy-pressure points at P = 0, and 10 GPa. (b) The phase diagram is simulated using DFT-PBE and vdW density functional of vdW-DF2. We used the Vinet EOS and six enthalpy-pressure points at P = 0, 2, 4, 6, 8, and 10 GPa.

(BO) approximation is used. According to BO approximation the electronic and nuclear wave functions can be separated. At the static level, it is also assumed that the nuclei are infinitely massive and the total nuclear momentum contribution in the Hamiltonian is zero. To find out the best candidate for Z=4 at the studied pressures, we used the PBE[49] and vdW-DF2[50] functionals to calculate the enthalpy difference between the *Pbca*, $P4_32_12$, and $P2_1/c$ structures. We performed calculations at six different volumes corresponding to DFT pressures of 0, 2, 4, 6, 8, and 10 GPa (Figure 7). Based on the linear fitting of the PBE results on two enthalpy-pressure points at P = 0 and 10 GPa, the *Pbca* structure is stable up to 3.6 GPa, whereas $P4_32_12$ is stable in the pressure range of 3.6−6.8 GPa, and finally the $P2_1/c$ structure has lowest enthalpy in pressures higher than 6.8 GPa.

A line between these two enthalpy-pressure points gives excellent agreement with the previous PBE computations by Wen *et al.*[2] (Fig. 2(a)). However we find this result to be inaccurate, and a denser set of points in this pressure range is needed.

Using the Vinet[51] equation of state (EOS) we found that the $P4_32_12$ structure is not stable in the pressure range of 0−10 GPa. The results of our EOS calculations are presented in figure 7. The enthalpy difference between the *Pbca*, $P4_32_12$, and $P2_1/c$ structures versus pressure is calculated using PBE and vdW-DF2[50] functionals (Figure 4(b)). The root-mean-
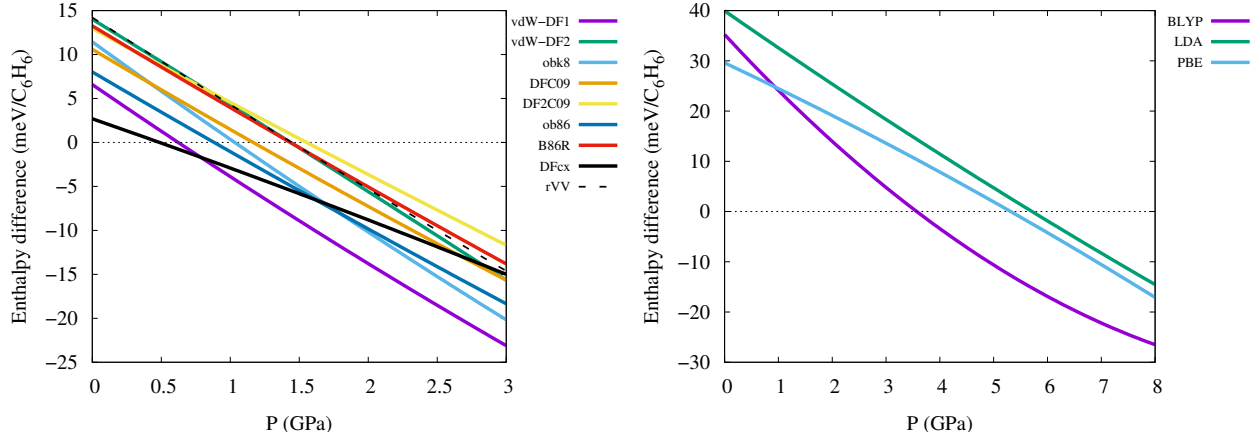
FIG. 5. (colour online) Enthalpy difference between $Pbca$ (phase I) and $P2_1/c$ (phase II) as function of pressure obtained with vdW and conventional DFT functionals. The left panel shows the results of vdW-DF1[52], vdW-DF2[50], rVV[56,57], obk8, B86R, ob86[35,53], DFCx[55], DFC09, and DF2C09[54] vdW functionals. The right panel illustrates the results of conventional DFT including PBE[49], LDA[58], and BLYP[59].

square deviation (RMSD) for PBE $- P2_1/c$ and PBE $- P4_32_12$ fittings are 0.0021 and 0.0019, respectively. The RMSD for vdW-DF2 $- P2_1/c$ and vdW-DF2 $- P4_32_12$ fittings are 0.0024 and 0.0026, respectively. We find that instability of $P4_32_12$ is independent of employed functional. Our results indicate that $Pbca$ and $P2_1/c$ are the most stable structures in the studied pressure ranges. These results are consistent with the experimental phase diagram proposed by Ciabini et $al.$[3,9-11]. Therefore, in the rest of this paper, we label $Pbca$ and $P2_1/c$ as phases I and II, respectively.

To study the importance of dispersion effects, we calculated the phase diagram of crystalline benzene using different functionals (Figure 5). We employed vdW-DF1[52], vdW-DF2[50], vdW-DF-obk8, vdW-DF-ob86, vdW-DF2-B86R[35,53], vdW-DF-C09, vdW-DF2-C09[54], vdW-DF-cx[55], and vdW-rVV[56,57] vdW functionals. Except rVV functional, the nonlocal term in the other vdW functionals is either vdW-DF1[52] or vdW-DF2[50]. Employing various gradient corrections to the exchange energy results in a variety of vdW functionals. We also determined the phase diagram using conventional DFT functionals, including PBE[49], LDA[58], and BLYP[59].

The vdW functionals yield different I−II phase transition pressure. Figure 6 illustrates $Pbca$ to $P2_1/c$ phase transition pressures which are obtained by different vdW functionals.
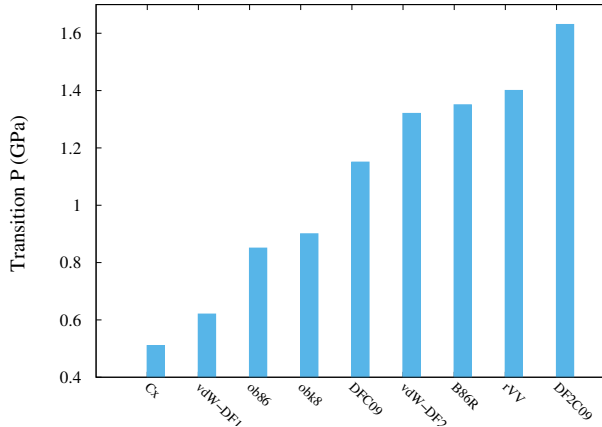
FIG. 6. (colour online) *Pbca* to $P2_1/c$ phase transition pressure. The results are calculated using different vdW functionals as explained in text.

The Cx[55] and DF2C09[54] functionals show the lowest and highest phase transition pressures, respectively. The difference between largest and smallest phase transition pressure is about 1.1 GPa. This value corresponds to inaccuracy in prediction of phase transition pressure by vdW functionals. It should be noted that the experimental *Pbca* to $P2_1/c$ phase transition occurs within 1.4 GPa pressure window. The results of the PBE, LDA, and BLYP functionals predict that the phase I−II transition occurs at 5.2, 5.6, and 3.5 GPa, respectively.

Our phase diagram calculations indicate that vdW results are in better agreement with experiments than the conventional functionals. Between the PBE and BLYP functionals, the PBE δ_{C-C} results are closer to vdW-DF1 and vdW-DF2 δ_{C-C} at low pressures. The difference between PBE phase transition pressure and vdW-DF1 and vdW-DF2 phase transition pressures are 4.55 and 3.9 GPa, respectively. However the difference between BLYP phase transition pressure and vdW-DF1 and vdW-DF2 phase transition pressures are 2.85 and 2.2 GPa, respectively. As we discussed in the previous section, vdW-DF1 and vdW-DF2 δ_{C-C} are positive for both *Pbca* and $P2_1/C$ structures below 2 GPa where the phase transition between them happens. Therefore the phase I−II transition in crystalline benzene occurs without any intermolecular contacts. This transition occurs only due to dispersion effects.

Using our DFT results we compute the EOS of *Pbca* and $P2_1/c$ structures. Figure 7 represents the results which are obtained by vdW and conventional functionals. We compare our DFT results with experiments which are reported in References 9 and 11. The experimental results in Ref. 9 are $V(P)$ data for crystalline benzene at 540 K that have been
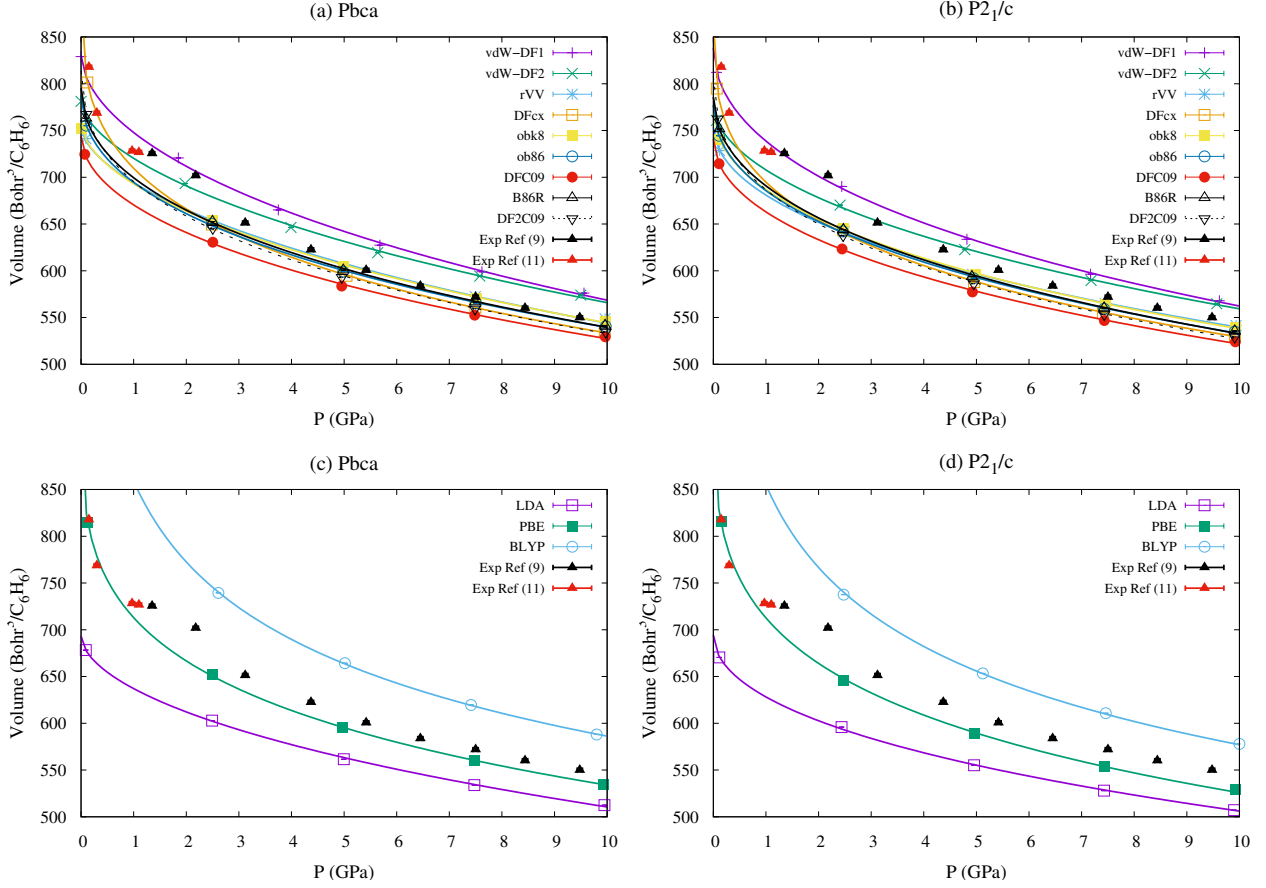
FIG. 7. (colour online) EOS of *Pbca* and $P2_1/c$ structures obtained by vdW ((a) and (b)) and conventional ((c) and (d)) DFT functionals. The results are compared with experimental data which are reported in References 9 and 11.

fitted by the Vinet EOS. The second experimental results[11] belong to crystalline benzene at lower pressures and 295 K. Among DFT conventional functionals used in this study only the PBE $V(P)$ results are close to experiments. The BLYP and LDA curves lie far above and below experimental curves, respectively. In general, the vdW results are in good agreement with experiments. At lower pressures vdW-DF1[52], vdW-DF2[50], and DFcx[55] $V(P)$ points for *Pbca* phase are close to experiments. With increasing the pressure, the $P2_1/c$ $V(P)$ curves computed with vdW-DF2[50], obk8[35,53], rVV[56,57], and B86R[35,53] are close to experimental points. The rVV functional has a different nonlocal correlation kernel, whereas other vdW functionals are the modified versions of vdW-DF1 or vdW-DF2. Our EOS calculations indicate that the modifications bring the vdW-DF1 and vdW-DF2 $V(P)$ curves below experimental ones. It is hard to conclude whether these modifications improve the accuracy of
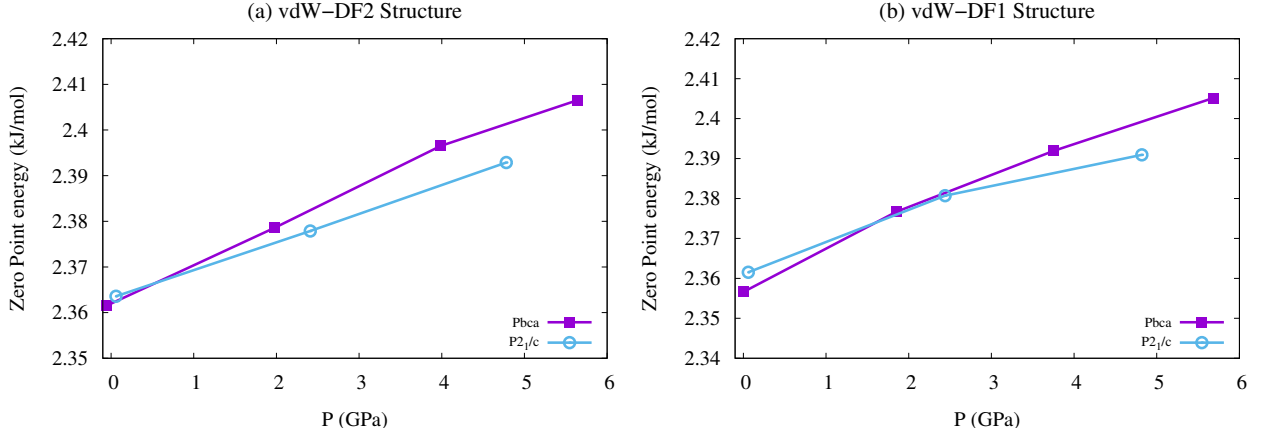
FIG. 8. (colour online) ZPE of *Pbca* and $P2_1/c$ structures obtained by DFT. Geometries are accurately optimised by two functionals: (a) vdW-DF2[50] and (b) vdW-DF1[52].

vdW-DF1 and vdW-DF2 fucntionals, especially in the case of vdW-DF2 fucntional, which overall gives the most accurate results. Our ground state EOS calculations indicate that at fixed pressure the volume per benzene molecule for *Pbca* phase is larger than $P2_1/c$. This is in agreement with finite temperature experimental measurements. This conclusion is also independent of used DFT functionals.

To investigate the ZPE contribution in phase diagram calculations, we simulated the difference between the gas and crystal ZPEs. The ZPE of the *Pbca* and $P2_1/c$ structures with respect to gas phase is shown as function of pressure (Figure 8). We used the vdW-DF2 and vdW-DF1 functionals to optimise the structures for phonon calculations. ZPE is obtained using quasi-harmonic approximation, as explained in the previous section. Within the studied pressure range, the difference between the ZPE of phases I and II is less than 2 meV/atom. The vdW-DF2 results indicate that the phase I−II ZPE transition happens at 0.6 GPa, whereas the vdW-DF1 results predict that the phase I−II ZPE transition occurs at 1.65 GPa (Figure 8). The difference between the ZPE of phases I and II increases with pressure. The ZPE correction to the cohesive energy of crystalline benzene was previously calculated[60]. They evaluated the ZPE using Γ-point harmonic frequencies at the PBE level. They found that the ZPE of the *Pbca* structure is 44 meV/molecule. In their calculations, they employed experimentally reported[61] orthorhombic cell without full three-dimensional optimisation. Finite-temperature experiments[62] show that the ZPE of crystalline benzene is 2.8 kJ/mol (29.02 meV/molecule). The ZPE experimental result is also employed to investi-
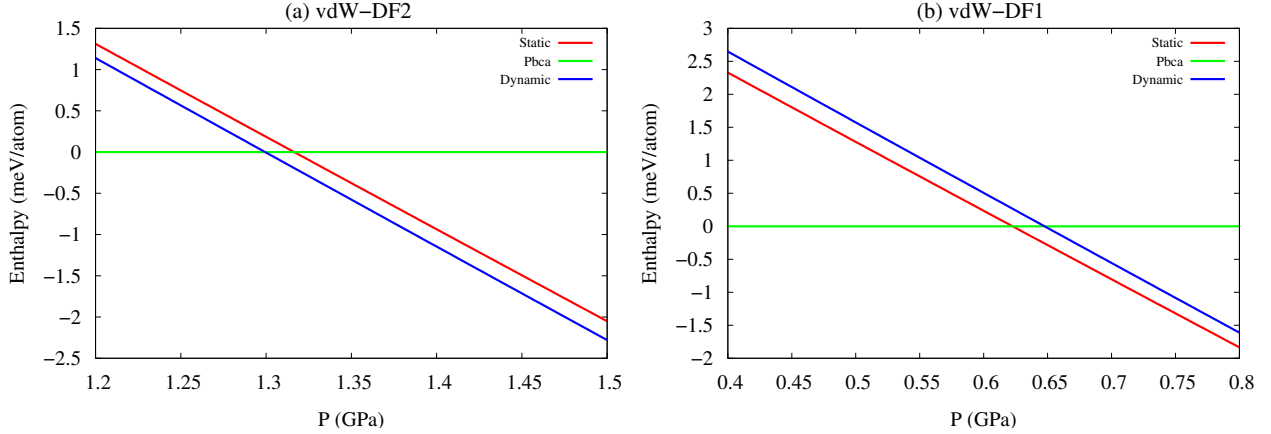
FIG. 9. (colour online) Static and dynamic phase transition of *Pbca* to *P*2$_1$/*c* obtained by (a) vdW-DF2[50] and (b) vdW-DF1[52] vdW functionals.

gate the binding energy of benzene crystal[63]. An estimate of 4.8 kJ/mol was obtained using DFT many-body dispersion method[64]. This ZPE is significantly larger than an estimate of 2.8 kJ/mol which is obtained by finite molecular cluster calculations[12,65]. Our ZPE results are close to PBC-DFT calculations[66], where an estimate of 2.6 kJ/mol is obtained using the PBE functional.

The static phase diagrams in Figure 5 assume that the atoms are infinitely massive. We calculate the dynamic phase diagram by adding the ZPE to the static results. Figure 9 illustrates the dynamic phase diagrams of crystalline benzene at the DFT level. The vdW-DF2 results indicate that adding ZPE lowers the phase transition by 0.02 GPa, and the *Pbca* to *P*2$_1$/*c* phase transition pressure is 1.42 GPa. The vdW-DF1 results predict that the phase transition occurs at 0.66 GPa, which is 0.03 GPa higher than the static phase transition pressure. The results of comparing the static and dynamic phase diagrams indicates that the ZPE contribution is negligible.

C. Finite Temperature DMC Phase Diagram

In this section we present our finite temperature phase diagram calculations. We use QMC based methods to calculate the electronic structure ground state energy. The inadequacy of mean-field-like DFT calculations of hydrogen-rich systems was demonstrated before[67]. To obtain reliable results, going beyond DFT-based methods and properly considering many-body effects are necessary. The DMC is generally considered as the most accu-

rate first-principle method available in studying the phase diagram of hydrogen-dominant materials[31,32]. In addition DMC is an effective method to study non-covalent systems. It can reach and go beyond the chemical accuracy which is desired for non-covalent systems[16].

We perform DMC calculations to obtain the wave-function-based phase diagram for crystalline benzene at low-pressures. We use the vdW-DF2 optimized structure for our DMC calculations. As we demonstrated in our DFT calculations, vdW-DF2 functional gives the closest results to experiment. The DMC results for energies in the limit of infinite system size are obtained by extrapolation using DMC energy data at $1 \times 1 \times 1$ and $2 \times 2 \times 2$ simulation cells.

TABLE I. DMC energies of the *Pbca* (phase I) structure. Energies are obtained at two simulation cells containing $N_1 = 48$ and $N_2 = 384$ atoms. Linear extrapolated energies are shown as $E(\infty)$. Energy (E) and volume (Vol) are in eV and Bohr^3 per benzene molecule, respectively.

Vol	$E(N_1)$	$E(N_2)$	$E(\infty)$
781.086	-1024.7464(4)	-1022.7063(8)	-1022.4140(8)
693.335	-1024.6376(5)	-1022.5976(7)	-1022.3052(7)
646.304	-1024.4880(5)	-1022.4478(5)	-1022.1556(5)
619.413	-1024.3588(4)	-1022.3185(5)	-1022.0264(5)

Table I lists the DMC energies of the *Pbca* structure at four primitive unit-cell volumes. We consider two simulation cells for each density containing 48 and 384 atoms. DMC energy at thermodynamic limit is obtained by linear extrapolation in $1/N$.

TABLE II. DMC energies of the $P2_1/c$ (phase II) structure. Energies are obtained at two simulation cells containing $N_1 = 24$ and $N_2 = 192$ atoms. Linear extrapolated energies are shown as $E(\infty)$. Energy (E) and volume (Vol) are in eV and Bohr^3 per benzene molecule, respectively.

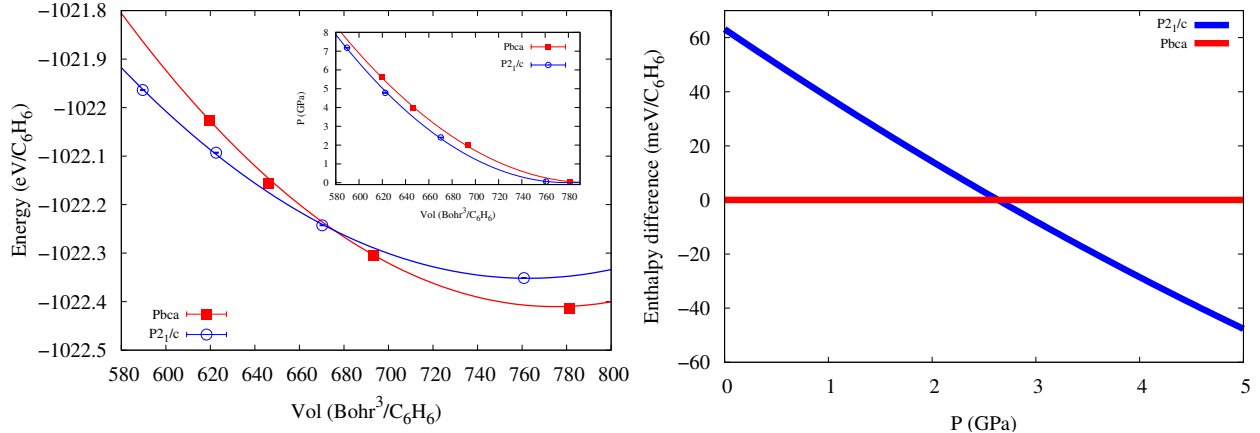| Vol	$E(N_1)$	$E(N_2)$	$E(\infty)$
760.8398	-1024.8824(5)	-1022.6683(8)	-1022.3514(8)
670.2382	-1024.7736(6)	-1022.5582(8)	-1022.2426(8)
622.5712	-1024.6240(5)	-1022.4099(7)	-1022.0929(8)
589.6330	-1024.4948(5)	-1022.2793(8)	-1021.9637(8)

FIG. 10. (colour online) (left) DMC energy of the *Pbca* and $P2_1/c$ structures as function of volume per benzene molecule. The inset shows the DMC pressure as function volume. Energy error bars are included in point sizes and are of the order of meV. (right) Relative enthalpies of the *Pbca* and $P2_1/c$ structures as function of pressure. The widths of the DMC lines indicate the estimated uncertainties in the enthalpies because of statistical and systematic errors.

Table II shows the DMC energies of the $P2_1/c$ structure at different primitive unit-cell volumes. We consider two simulation cells for each density containing 24 and 192 atoms. DMC energy at infinite system size limit is calculated by linear extrapolation in $1/N$.

To identify enthalpy-pressure curves for the *Pbca* and $P2_1/c$ structures, we fitted model equations of state $E(V)$ to our finite-size-corrected DMC energy against volume V. We used the Vinet EOS[51] to fit our total energies and propagate errors using classical statistics. The pressure $P = -(\partial E/\partial V)$ and the enthalpy is $H = E + PV$, where E is DMC electronic structure energy of system.

Figure 10 (left) illustrates the DMC energy of phases I and II of crystalline benzene as function of volume per benzene molecule. The inset illustrates the DMC pressure as function of volume for *Pbca* and $P2_1/c$ structures. With increasing density, phase II becomes favourable over phase I in the *Pbca* structure. Figure 10 (right) shows the relative enthalpies of the *Pbca* and $P2_1/c$ structures. Based on our static enthalpy-pressure phase diagram, the *Pbca* to $P2_1/c$ phase transition occurs at pressure 2.6±0.1 GPa. The use of the DMC method has significant consequences for the static-lattice relative enthalpies of the studied structures. Compared with vdW-DF2, the DMC enthalpy-pressure results predict that the phase I−II transition occurs at 1.2 GPa higher pressure. Among conventional DFT functionals, the
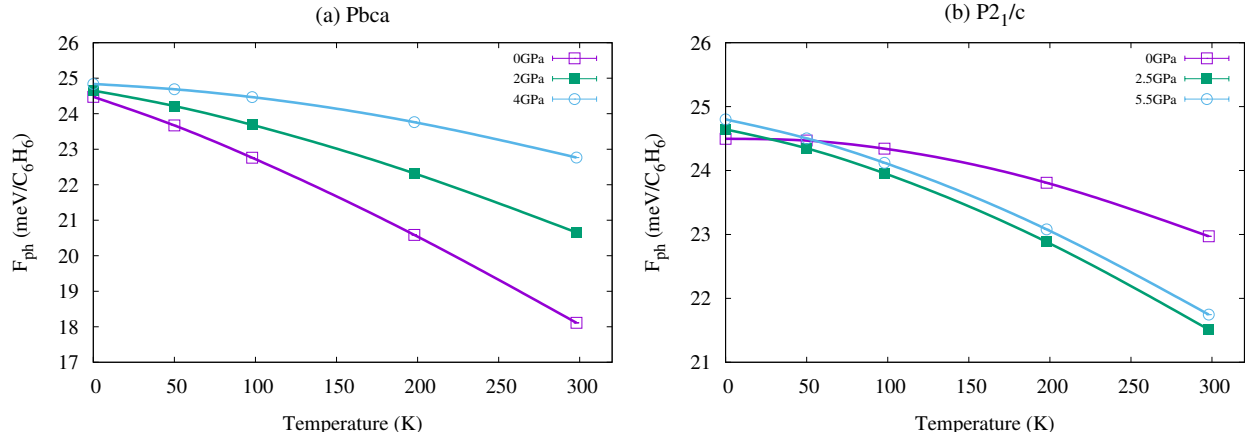
16

FIG. 11. Phonon contribution to the Helmholtz free energies F_{ph} of the $Pbca$ and $P2_1/c$ structures of crystalline benzene. The geometries are optimized using vdW-DF2[50] functionals.

BLYP results are closest to DMC. The difference between DMC and BLYP phase transition pressure is 0.9 GPa.

To obtain the phase diagram at finite temperature, we used quasi-harmonic approximation to obtain lattice dynamic contribution to the free energies. Phonons have contributed to the Helmholtz free energies F_{ph} of crystalline benzene (Figure 11). We used vdW-DF2 functionals to optimise the $Pbca$ and $P2_1/c$ structures at different pressures. Vibrational free energies are calculated at different temperatures of 50, 100, 200, and 300 K. At room temperature and 0 GPa vibrational free energy of $P2_1/c$ is higher than $Pbca$. Meanwhile, the vibrational free energies of $Pbca$ become higher than $P2_1/c$ by increasing the pressure. This results indicates the stability of the $Pbca$ phase at ambient conditions, which is also observed experimentally[9,10].

We calculated relative Gibbs free energies of the $Pbca$ and $P2_1/c$ structures at room temperature (Figure 12). The static electronic structure results are obtained by DMC calculations. Our results predict that the room temperature $Pbca$ to $P2_1/c$ structure transformation happens at 2.1(1) GPa. Experiments indicate that the room temperature phase transition of $Pbca$ to $P2_1/c$ occurs at around 1.4 GPa[3]. The I to II phase transition is a temperature dependent transformation, and it can be speeded up by heating the sample[1]. Keeping the low-pressure phase I, $Pbca$, in a metastable state at least up to 3 GPa is possible without heating[5]. Our zero temperature DMC phase diagram predicts that the $Pbca$ phase could be stable up to 2.6(1) GPa (Figure 12(a)). The phase diagram that we have obtained by combining DMC static-lattice energies and quasi-harmonic vibrational energies can be
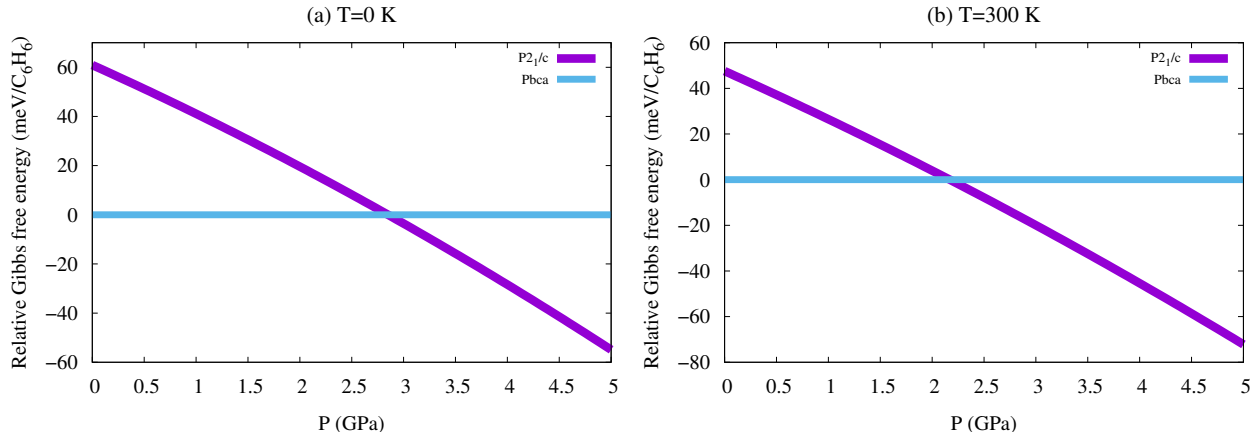
FIG. 12. Relative Gibbs free energies of the *Pbca* and $P2_1/ca$ structures. (a) 0 K, and (b) 300 K. The Gibbs free energies are calculated using static-lattice DMC calculations together with DFT quasi-harmonic vibrational calculations.

extended to higher pressures.

As the final step of our study, we calculated the lattice energy of crystalline benzene at ambient conditions. The cohesive energy yields the strength of the vdW forces holding the crystalline benzene together. We used our DMC and ZP energies for *Pbca* structure. The cohesive energy is calculated using the difference between total energies of *Pbca* structure and its fragments. Cohesive energy calculation is a precise test of DMC method, since it has to accurately describe two different systems of benzene molecule and crystalline benzene. The electronic structure of these two systems are not similar. In our DMC lattice energy calculation, we used same time step of 0.01 a.u for both crystal and molecule. We found an estimate of 50.6±0.5 kJ/mol for lattice energy. Ab initio many-electron wave functions methods provide an estimate of 55.90±0.76 kJ/mol for benzene crystal lattice energy at zero temperature[15]. The experimental lattice energy at same condition is 55.3±2.2 kJ/mol[15]. We used conventional Jastrow factor in our DMC calculations. In principle, the DMC lattice energy can be systematically improved by accurately taking into account the correlation energy and also decreasing the fixed-node errors. These purposes can be fulfilled by adding additional terms in Jastrow factor and using backflow transformations[16]. However, improving the DMC lattice energy until it converges to exact results requires huge amount of computational time.

IV. CONCLUSION

We have comprehensively studied the crystalline benzene phase diagram at pressures below 10 GPa. We have used different vdW functionals and also three most used conventional functionals to obtain DFT energy of system. The vdW-DF2 results of our study indicated that the *Pbca* and $P2_1/c$ structures are the best candidates for phases I and II, respectively. We have used the accurate DMC method to calculate the ground-state electronic structure energy of system. We have compared static enthalpy-pressure phase diagrams which are obtained by DFT and DMC methods. We used quasi-harmonic approximation and density functional perturbation theory to calculate the phonon contribution to the free energy of system. Our Gibbs free energy phase diagram predicts that at room temperature, the phase I−II transition occurs at 2.1(1) GPa, which is 0.7(1) GPa higher that experimental result[3]. Our DMC energies at the thermodynamic limit are calculated using $1 \times 1 \times 1$ and $2 \times 2 \times 2$ cell extrapolation. Improving the finite size extrapolation may reduce the difference between our DMC Gibbs free energy and experiment. The other source of this difference could be the quasi-harmonic approximation which has been used in this work. Anharmonic contribution plays an important role in the study of phase diagram of hydrogen-dominant materials and can affects the phase transition pressure[31,32]. We have found DMC lattice energy of 50.6±0.5 kJ/mol for crystalline benzene at ambient conditions. The results of our study indicate the importance of many-body electronic structure calculation to obtain a reliable phase diagram for molecular crystals.

knowledges the support of the Carnegie Institution for Science

---

[1] M. M. Thièry and J. M. Lèger, J. Chem. Phys. **89**, 4255 (1988).

[2] X.-D. Wen, R. Hoffmann, and N. W. Ashcroft, J. Am. Chem. Soc. **133**, 9023 (2011).

[3] G. J. Piermarini, A. D. Mighell, C. Weir, and S. Block, Science **165**, 3461 (1969).

[4] P. Raiteri, R. Martonak, and M. Parrinello, Angew. Chem. Int. Ed. **44**, 3769 (2005).

[5] P. W. Bridgman, J. Chem. Phys **9**, 794 (1941).

[6] E. G. Cox and J. A. S. Smith, Nature **173**, 75 (1954).

[7] E. G. Cox, D. W. Cruickshank, and J. A. S. Smith, Proc. R. Soc. London A **247**, 1 (1958).

[8] G. E. Bacon, N. A. Curry, and S. A. Wilson, Proc. R. Soc. A **279**, 98 (1964).

[9] L. Ciabini, F. A. Gorelli, M. Santoro, R. Bini, V. Schettino, and M. Mezouar, Phys. Rev. B **72**, 094108 (2005).

[10] L. Ciabini, M. Santoro, F. A. Gorelli, R. Bini, V. Schettino, and S. Raugei, Nature Mater. **6**, 39 (2007).

[11] A. Katrusiak, M. Podsiadzo, and A. Budzianowski, Crystal Growth & Design **10**, 3461 (2010).

[12] R. Podeszwa, B. M. Rice, and K. Szalewicz, Phys. Rev. Lett. **101**, 115503 (2008).

[13] S. Grimme, J. Antony, S. Ehrlich, and H. Krieg, J. Chem. Phys. **132**, 154104 (2010).

[14] J. P. Perdew, K. Burke, and M. Ernzerhof, Phys. Rev. Lett. **77**, 3865 (1996).

[15] J. Yang, W. Hu, D. Usvyat, D. Matthews, M. Schutz, and G. K.-L. Chan, Science **345**, 640 (2014).

[16] S. Azadi and R. E. Cohen, J. Chem. Phys. **143**, 104301 (2015).

[17] W. M. C. Foulkes, L. Mitas, R. J. Needs, and G. Rajagopal, Rev. Mod. Phys. **73**, 33 (2001).

[18] M. Marchi, S. Azadi, M. Casula, and S. Sorella, J. Chem. Phys. **131**, 154116 (2009).

[19] M. D. Brown, J. R. Trail, P. L. Ríos, and R. J. Needs, J. Chem. Phys. **126**, 224110 (2007).

[20] I. G. Gurtubay and R. J. Needs, J. Chem. Phys. **127**, 124306 (2007).

[21] J. R. Trail and R. J. Needs, J. Chem. Phys. **128**, 204103 (2008).

[22] S. Azadi, R. Singh, and T. D. Kuhne, Int. J. Quantum Chem. **115**, DOI: 10.1002/qua.25005 (2015).

[23] M. Marchi, S. Azadi, and S. Sorella, Phys. Rev. Lett. **107**, 086807 (2011).

[24] E. Mostaani, N. Drummond, and V. Falḱo, Phys. Rev. Lett. **115**, 115501 (2015).

[25] S. Azadi and W. M. C. Foulkes, J. Chem. Phys. **143**, 102807 (2015).

[26] S. J. Cox, M. D. Towler, D. Alfè, and A. Michaelides, J. Chem. Phys. **140**, 174703 (2014).

[27] J. Ma, A. Michaelides, and D. Alfè, J. Chem. Phys. **134**, 134701 (2011).

[28] Y. S. Al-Hamdani, D. Alfè, and O. A. von Lilienfeld, J. Chem. Phys. **141**, 18C530 (2014).

[29] N. A. Benedek, I. K. Snook, M. D. Towler, and R. J. Needs, J. Chem. Phys. **125**, 104302 (2006).

[30] M. Dubecký, L. Mitas, and P. Jurečka, Chem. Rev. **116**, 5188 (2016).

[31] N. Drummond, B. Monserrat, J. Lloyd-Williams, P. L. Rìos, and R. J. Needs, Nature Communications **6**, 7749 (2015).

[32] S. Azadi, B. Monserrat, W. M. C. Foulkes, and R. J. Needs, Phys. Rev. Lett. **112**, 165501 (2014).

[33] S. Azadi, W. M. C. Foulkes, and T. D. Kuhne, New Journal of Physics **15**, 113005 (2013).

[34] E. Miliordos, E. Aprà, and S. S. Xantheas, J. Phys. Chem. A **118**, 7568 (2014).

[35] J. Klimeš and A. Michaelides, J. Chem. Phys. **137**, 120901 (2012).

[36] P. G. *et al.*, J. Phys.: Condens. Matter **21**, 395502 (2009).

[37] A. M. Rappe, K. M. Rabe, E. Kaxiras, and J. D. Joannopoulos, Phys. Rev. B **41**, 1227 (1990).

[38] S. Baroni, S. de Gironcoli, and A. D. Corso, Rev. Mod. Phys. **73**, 515 (2001).

[39] R. J. Needs, M. D. Towler, N. D. Drummond, and P. L. Ríos, J. Phys.: Condens. Matter **22**, 023201 (2010).

[40] J. R. Trail and R. J. Needs, J. Chem. Phys. **122**, 174109 (2005).

[41] J. R. Trail and R. J. Needs, J. Chem. Phys. **122**, 014112 (2005).

[42] L. Mitas, E. L. Shirley, and D. M. Ceperley, J. Chem. Phys. **95**, 3467 (1991).

[43] C. W. Greeff and W. A. L. Jr., J. Chem. Phys. **109**, 1607 (1998).

[44] J. M. Zuo, P. Blaha, and K. Schwarz, J. Phys.: Condens. Matter **9**, 7541 (1997).

[45] S. Azadi, C. Cavazzoni, and S. Sorella, Phys. Rev. B **82**, 125112 (2010).

[46] D. Alfè and M. J. Gillan, Phys. Rev. B **70**, 161101 (2004).

[47] C. J. Umrigar, K. G. Wilson, and J. W. Wilkins, Phys. Rev. Lett. **60**, 1719 (1988).

[48] N. D. Drummond and R. J. Needs, Phys. Rev. B **72**, 085124 (2005).

[49] J. Perdew, A. Ruzsinszky, G. I. Csonka, O. A. Vydrov, G. E. Scuseria, L. A. Constantin, X. Zhou, and K. Burke, Phys. Rev. Lett. **100**, 136406 (2008).

[50] K. Lee, E. D. Murray, L. Kong, B. I. Lundqvist, and D. C. Langreth, Phys. Rev. B **82**, 081101(R) (2010).

[51] P. Vinet, J. Ferrante, J. R. Smith, and J. H. Rose, J. Phys. C Solid State **19**, L467 (1986).

[52] M. Dion, H. Rydberg, E. Schröder, D. C. Langreth, and B. I. Lundqvist, Phys. Rev. Lett. **92**, 246401 (2004).

[53] J. Klimeš, D. R. Bowler, and A. Michaelides, Phys. Rev. B **83**, 195131 (2012).

[54] V. R. Cooper, Phys. Rev. B **89**, 035412 (2010).

[55] K. Berland and P. Hyldgaard, Phys. Rev. B **89**, 035412 (2014).

[56] R. Sabatini, T. Gorni, and S. de Gironcoli, Phys. Rev. B **87**, 041108(R) (2013).

[57] O. A. Vydrova and T. V. Voorhis, J. Chem. Phys. **133**, 244103 (2010).

[58] J. P. Perdew and A. Zunger, Phys. Rev. B **23**, 5048 (1981).

[59] C. Lee, W. Yang, and R. G. Parr, Phys. Rev. B **37**, 785 (1988).

[60] O. Bludský and M. Rubeš, Phys. Rev. B **77**, 092103 (2008).

[61] W. I. F. David, R. M. Ibberson, G. A. Jeffrey, and J. R. Ruble, Physica B **180**, 597 (1992).

[62] M. Nakamura and T. Miyazawa, J. Chem. Phys. **51**, 3146 (1969).

[63] D. Lu, Y. Li, D. Rocca, and G. Galli, Phys. Rev. Lett. **102**, 206411 (2009).

[64] A. M. Reilly and A. Tkatchenko, J. Chem. Phys. **139**, 024705 (2013).

[65] A. L. Ringer and C. D. Sherrill, Chemistry **14**, 2542 (2008).

[66] A. O. de-la Roza and E. R. Johnson, J. Chem. Phys. **137**, 054103 (2012).

[67] S. Azadi and W. M. C. Foulkes, Phys. Rev. B **88**, 014115 (2013).

[68] N. D. Drummond, R. J. Needs, A. Sorouri, and W. M. C. Foulkes, Phys. Rev. B **78**, 125106 (2008).